Can an inorganic coating serve as stable SEI for aqueous superconcentrated electrolytes?

Léa Droguet,[a,b,c,$] Gustavo M. Hobold,[d,$] Marie Francine Lagadec,[a,c], Rui Guo,[d] Christophe Lethien,[c,e] Maxime Hallot,[c,e] Olivier Fontaine,[c,f] Jean-Marie Tarascon,[a,b,c] Betar M. Gallant[d] and Alexis Grimaud[a,b,c]**

[a] Chimie du Solide et de l'Energie, UMR 8260, Collège de France, 11 place Marcelin Berthelot, 75231 Paris Cedex 05, France

[b] Sorbonne Université, 4 place Jussieu, 75005 Paris, France

[c] Réseau sur le stockage Electrochimique de l'Energie (RS2E), CNRS FR3459, 33 rue Saint Leu, 80039 Amiens Cedex, France

[d] Department of Mechanical Engineering, Massachusetts Institute of Technology, Cambridge, MA 02139

[e] Université de Lille, CNRS, Centrale Lille, Université Polytechnique Hauts-de-France, UMR 8520 - IEMN, F-59000 Lille, France

[f] Institut Charles Gerhardt Montpellier, Université Montpellier, UMR 5253, Place Eugène Bataillon, 34095 Montpellier, France

[$] L.D. and G.M.H. contributed equally to this paper

Corresponding Authors

Alexis Grimaud: alexis.grimaud@college-de-france.fr

Betar M. Gallant: bgallant@mit.edu

Abstract

Developing a stable, conformal solid electrolyte interphase (SEI) for aqueous-based Li-ion batteries has been a long-awaited dream to support the development of non-toxic and eco-friendly energy storage technologies. Toward that goal, aqueous superconcentrated electrolytes were recently introduced as their unique solvation structure allows for forming a LiF-rich SEI layer at the negative electrode, imparting the stability to the interface. However, the intrinsic stability of such LiF-rich SEI was never measured, despite growing evidences of poor passivation properties and water reduction upon operation. In this work, LiF conformal layers were coated onto lithium electrodes and their reactivity towards superconcentrated aqueous electrolytes studied by combining solubility measurements, *in situ* microscopy and gas chromatography. We demonstrate that the use of superconcentrated electrolytes drastically reduces the solubility of LiF. However, such layer is intrinsically unstable in aqueous environments, whilst stable in organic electrolytes, owing to the absence of self-passivation. Comparing different interfaces, we conclude that an artificial SEI made of an inorganic coating is not suitable for preventing water reactivity in aqueous systems.

TOC GRAPHICS

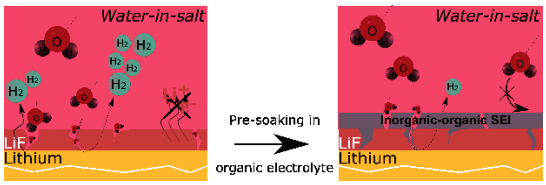

The deployment of Li-ion battery (LIB) technology beyond its initial purpose (portable electronics) to powering electric vehicles and storing electricity in the grid makes recyclability and sustainability major drivers for future research and development. In this spirit, replacing organic solvents – known for their volatility and toxicity – utilized in today's liquid LIB aprotic electrolytes with water appears as a promising strategy [1,2]. However, aqueous LIB have not yet materialized commercially because of their poor energy density, which is limited by the narrow electrochemical stability window for water (1.23 V at room temperature), and more precisely by water reduction. While limitations are also found regarding the reductive stability of classical organic electrolytes, no stable solid electrolyte interphase (SEI) components are formed in conventional (dilute) aqueous electrolytes unlike in carbonate-based electrolytes.

Therefore, developing stable SEIs in aqueous media has been at the forefront of research for aqueous Li-ion batteries and other aqueous technologies such as electrochemical capacitors (based on carbon or pseudocapacitive electrodes) or Na-ion batteries[1–4]. One major advance was the introduction of superconcentrated aqueous electrolytes in which the salt molecules outweigh the water molecules both in volume and in mass. Indeed, in these so-called "water-in-salt electrolytes" (WiSE)[1] or "water-in-bisalt electrolytes" (WiBS)[2,5], almost all water molecules contribute to the solvation sphere of Li^+, allowing for a strong ion-pair interaction between solvated Li^+ cations and organic anions such as bis(trifluoromethane)sulfonimide ($TFSI^-$) or its derivatives. While it has been established that this atypical solvation structure does not suppress the reduction of water at the negative electrode, it unlocks the reactivity of the $-CF_3$ terminal groups of $TFSI^-$ anions present at the interface and triggers the formation of LiF, which was suggested to passivate the negative electrode[6–9]. Hence, for organic LiB electrolytes, the decomposition of both the solvent molecules and salt anions results in a native SEI layer containing both inorganic (LiF, Li_2CO_3, Li_2O, etc.) and

organic/oligomeric species[10,11], for superconcentrated aqueous electrolytes the passivation instead predominantly relies on LiF.

While the prospect of widening the electrochemical stability window of water is promising, recent studies have reported a capacity loss and open circuit voltage decay corresponding to a slow but continuous self-discharge for Li-ion batteries using superconcentrated aqueous electrolytes[12,13]. This self-discharge is associated with the reduction of water and the evolution of hydrogen at the negative electrode (Mo_6S_8 for instance) when stored in a fully charged state according to the following reaction:

$$Li_4Mo_6S_8 + x \cdot H_2O \rightarrow Li_{4-x}Mo_6S_8 + x \cdot Li^+ + x \cdot HO^- + \frac{x}{2} \cdot H_2$$

However, the SEI thickness and density generally vary with the formation step (cycling rate, duration, temperature etc.). Equally, part of the SEI can be partially dissolved. This raises the question of whether the self-discharge originates from the morphology and porosity of the deposited LiF layer or from its intrinsic solubility and/or instability in WiSE. To decide between these two options, we first assessed the LiF solubility in aqueous electrolytes as a function of salt concentration. Then, we studied the stability of a conformal LiF layer deposited onto metallic Li anode as a proxy to mimic the formation of a native SEI. We then tested its stability against two WiSEs (20 m LiTFSI and 20 m LiTFSI : 8 m LiBETI) using gas chromatography. Combining these results and comparing them with those obtained in organic electrolytes, we conclude on the partially-protective role of both native and artificial LiF-rich SEI for superconcentrated aqueous electrolytes. More importantly, we demonstrate that a salt-derived inorganic and solvent-derived organic layers play a crucial role in the SEI's ability to self-repair and allow for cycling anode material outside of the thermodynamic stability window of the electrolyte.

The solubility limit of lithium fluoride is well-known in pure solvents.[14] It is notably greater in water than in most carbonate solvents, with the exception of EC (see Table S1). Very little is however

known regarding the solubility limit of LiF as a function of salt concentration, but the common-ion effect arising from the dissolved Li-salt is believed to lower the solubility of LiF in superconcentrated aqueous electrolytes. In order to probe this effect, the solubility limit of LiF was directly measured in aqueous electrolytes as a function of the LiTFSI salt concentration using a fluoride ion selective electrode (ISE) and following the protocol developed by Strmcnik *et al.* [15] (Figure 1a).

The LiF solubility limit was observed to decrease from pure water (0.93 g / L) down to 1.9 10^{-3} and 1.5 10^{-3} g / L for 20 m LiTFSI and 20 m LiTFSI : 8 m LiBETI aqueous electrolytes at 23 °C, respectively (Figure 1b). Considering the solubility reaction:

$$LiF_{(s)} = Li^{+}{}_{(aq)} + F^{-}{}_{(aq)} \quad (1)$$

the fluoride concentration in solution may be expressed as follows (see Supporting information for detailed calculations):

$$[F^{-}] = \frac{K_S}{\gamma^2_{Li^+F^-} \cdot [Li^+]_{electrolyte}} \quad (2)$$

with Ks the constant of solubility, $\gamma_{Li^+F^-}$ the activity coefficient of the LiF salt and $[Li^+]_{electrolyte}$ the initial concentration of lithium in the electrolyte. As theoretically described by McEldrew *et* al.[16], the logarithm of the activity coefficient $\log(\gamma_{Li^+F^-})$ increases with the molality. Therefore, even without knowing the effect of the molality and thus of the solvation structure on Ks, the decrease of solubility limit observed in *Figure 1*b is consistent with the common ion effect and the increase of activity coefficient, which are both related to the increase of molality.

a

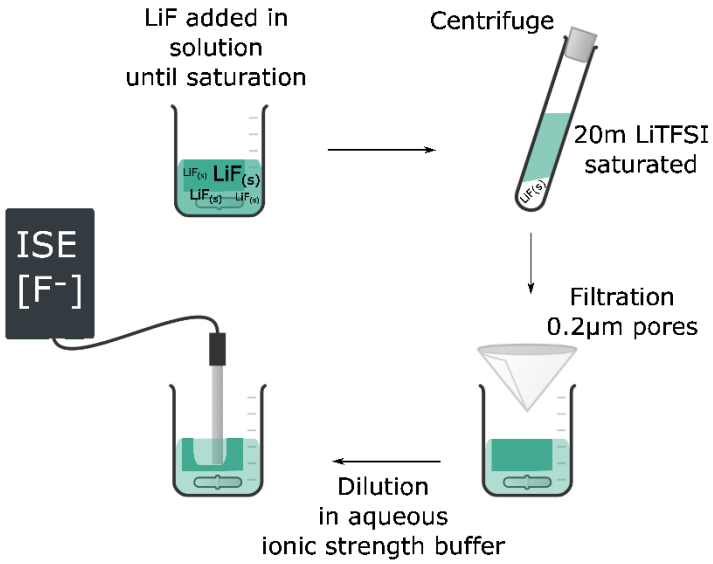
LiF added in solution until saturation
Centrifuge
20m LiTFSI saturated
Filtration 0.2µm pores
ISE [F⁻]
Dilution in aqueous ionic strength buffer

b

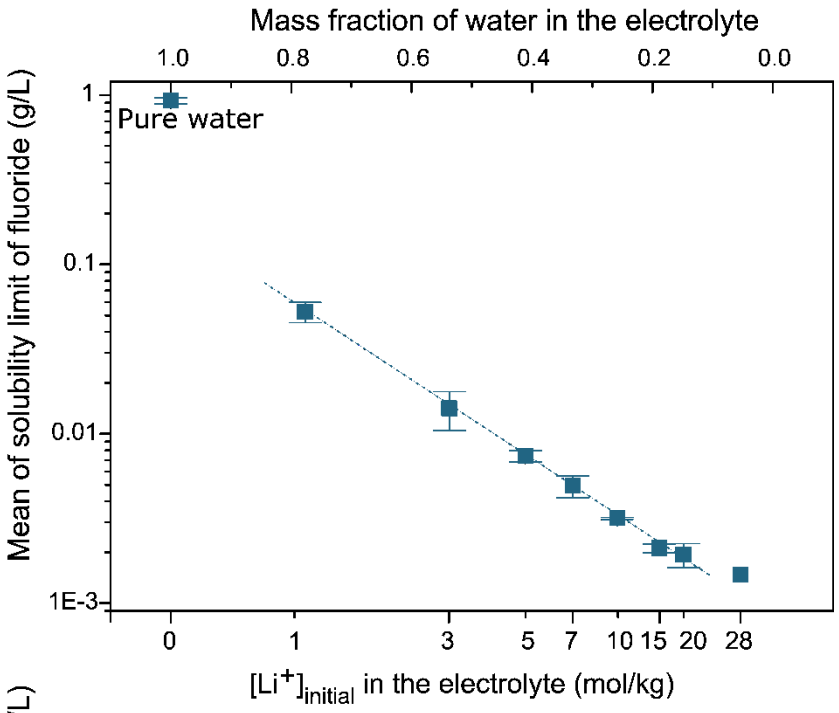
Mass fraction of water in the electrolyte
1.0
0.8
0.6
0.4
0.2
0.0
Pure water
Mean of solubility limit of fluoride (g/L)
1
0.1
0.01
1E-3
0
1
3
5
7
10
15
20
28
[Li+]initial in the electrolyte (mol/kg)

c

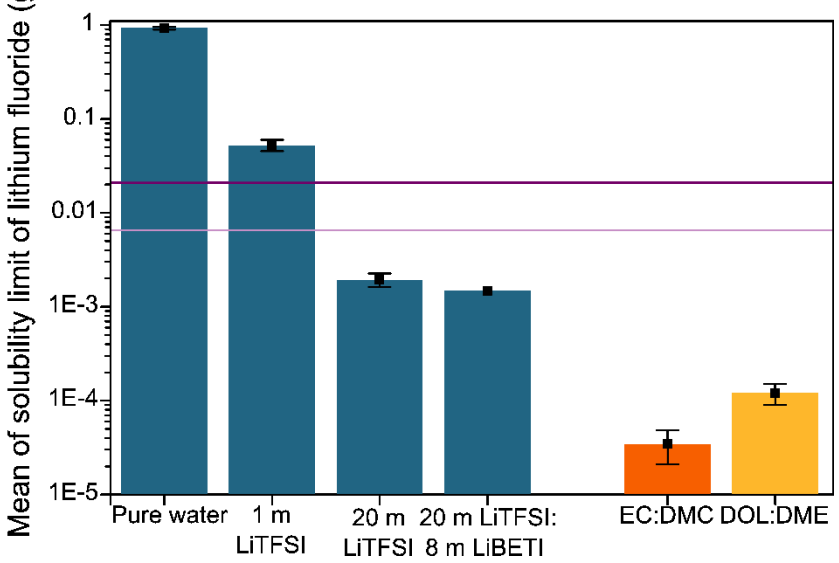
Mean of solubility limit of lithium fluoride (g/L)
1
0.1
0.01
1E-3
1E-4
1E-5
Pure water
1 m LiTFSI
20 m LiTFSI
20 m LiTFSI: 8 m LiBETI
EC:DMC
DOL:DME

Figure 1. (a) Schematic explanation of the protocol used to measure LiF solubility, further details are provided in the Supporting information. (b) Solubility limit of LiF in saturated aqueous solutions measured at different LiTFSI concentration ranging from 1m to 20m (WiSE) as well as for 20 m LiTFSI : 8 m LiBETI (WiBS). The dashed line is a guide to the eyes. (c) Comparison of the LiF solubility limits measured in different electrolytes: water, 1 m LiTFSI, 20 m LiTFSI, 20 m LiTFSI : 8 m LiBETI, EC:DMC (1:1 vol%), DOL/DME (1:1 vol%). The reference lines indicate the fluoride concentration expected from the complete dissolution of a 0.9 cm diameter and 30 nm thickness layer (dark purple, 2.02 . 10^{-2} g / L) or a 10 nm thickness (light purple, 6.72 . 10^{-3} g / L) LiF layer dissolved in 250 µL of electrolyte.

Having established that the LiF solubility limit is drastically decreased in WiSE, we focused our attention on the ability for LiF to protect a negative electrode against reacting with water. For that, a ~30 nm thick LiF coating was prepared by the reaction of NF_3 gas with a Li metallic anode under mild conditions, as previously demonstrated[17], to mimic the native LiF-rich SEI formed on the surface of anode materials in WiSE. Because of practical considerations in terms of energy density gain, we focused our attention on metallic Li anode rather than on the classically used Mo_6S_8 anodes, bearing in mind that the kinetics for electrolyte reduction will be greatly enhanced together with accompanied gas generation. Hence, it provides an accelerated approach to pinpoint the weaknesses of any SEI layer composed of LiF which will eventually appear during cycling of anode materials. During the Li/LiF sample preparation, the metallic Li is rolled on a current collector and then exposed to NF_3 gas at 175 °C, just below the melting temperature of Li, forming a complete LiF coating which protects the metallic Li when further exposed to moisture or electrolytes. Figure 1c compares the solubility limit of LiF in aqueous and organic electrolytes with the concentration of fluoride calculated for the complete dissolution of the 30 nm conformal LiF-layer in 250 µL of electrolyte, i.e. a concentration of fluoride of $2.02 \cdot 10^{-2}$ g / L. Doing so, one can infer that in diluted aqueous electrolytes, the conformal LiF-layer would fully dissolve in contrast to superconcentrated aqueous electrolyte. This trend is also preserved at 55°C since the LiF solubility increases but by less than a factor of 2 ($3.7 \pm 0.4 \cdot 10^{-3}$ g / L in WiSE and $2.9 \cdot 10^{-3}$ g / L in WiBS), so the very limited

dissolution still enables practical cycling conditions. This implies that the instability of the LiF-based SEI in WiSE should not arise from the dissolution of the passivating layer.

Having established that LiF solubility drastically decreased in WiSE, environmental scanning electron microscopy (E-SEM) was used to assess the protective power of the LiF layer against moisture (Figure 2). In this experiment, the sample is kept at 20°C while gradually increasing the relative humidity (RH) of the atmosphere in the chamber from 0 to 90 % (Figure 2a). As depicted in Figure 2b, round-shaped particles start forming on the surface of a metallic Li sample as the chamber's RH exceeds 0 %, their occurrence increasing with the increasing RH. On the contrary the LiF-conformal layer protects the metallic Li from reacting with gaseous water below a threshold of 60 % RH. However, approaching water condensation (RH ≈ 90 %), the LiF-conformal layer no longer plays a protective role and similar (but larger) round-shaped particles are observed alike for bare metallic Li. Interestingly, as observed in Figure 2b and illustrated in Figure 2c, reactivity can first be observed at cracks and pits formed in the LiF layer, suggesting that microstructural defects in the artificial SEI lead to reactions of the underneath Li layer with moisture.

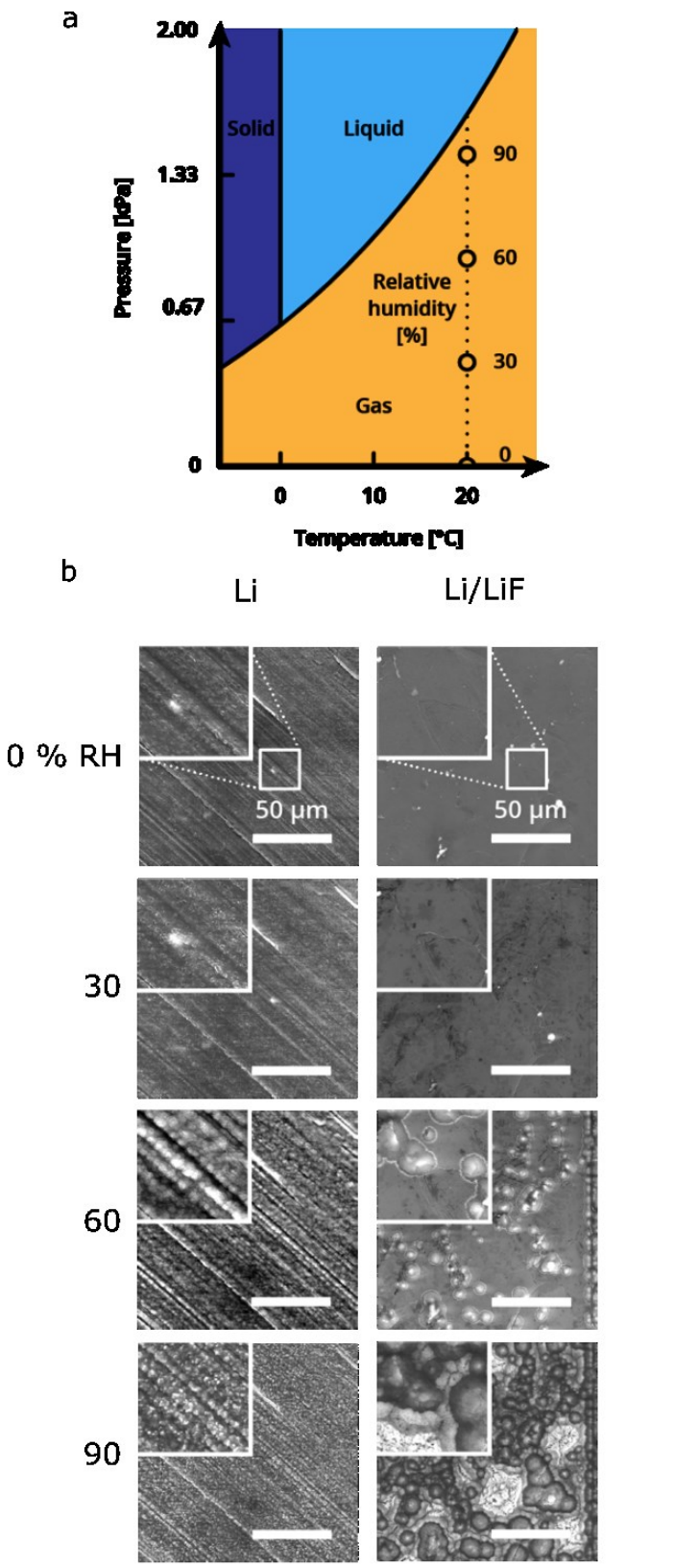
a
2.00
1.33
0.67
0
Pressure [kPa]
Solid
Liquid
Relative humidity [%]
Gas
90
60
30
0
0
10
20
Temperature [°C]
b
Li
Li/LiF
0 % RH
30
60
90
50 µm
50 µm
c
Ideal SEI
Real SEI
LiF
30nm*
Lithium
100µm
*: as observed by SEM
Lithium
H2

Figure 2. (a) Phase diagram for pure water and (b) E-SEM images for bare metallic Li (left) and LiF-protected metallic Li (right) taken successively at 0, 30, 60 and 90 % relative humidity (RH) with zoom-in. (c) Scheme of an ideal and a real SEI exposed to water.

Our attention then turned to the chemical stability of the LiF-coated metallic Li samples in both superconcentrated electrolytes. For that, LiF-protected Li samples were exposed to various electrolytes while monitoring the gas evolution by gas chromatography with thermal conductivity/flame ionization detectors (GC-TCD/FID) (see Figure 3). First, for comparative purposes, we determine the gas evolution when a LiF-protected Li sample is exposed to organic LP30 electrolyte (Figure 3a and Figure S 2). The total amount of gas released, well-known to originate from the decomposition of carbonates (*i.e.* CO, CO_2, C_2H_4 and CH_4), stabilizes after 30 minutes at a very low value of approximately $0.5 \cdot 10^{-2}$ % in the headspace (the rest being argon), which is close to the detection limit of the GC-FID instrumentation. Hence, even though minute cracks exist in the LiF-conformal layer, the exposition of bare Li to LP30 eventually leads to the formation of some polymeric/oligomeric structures that passivate the electrode[18,19] and prevent further gas evolution, explaining the decrease of gas detected over time (inset in Figure 3a).

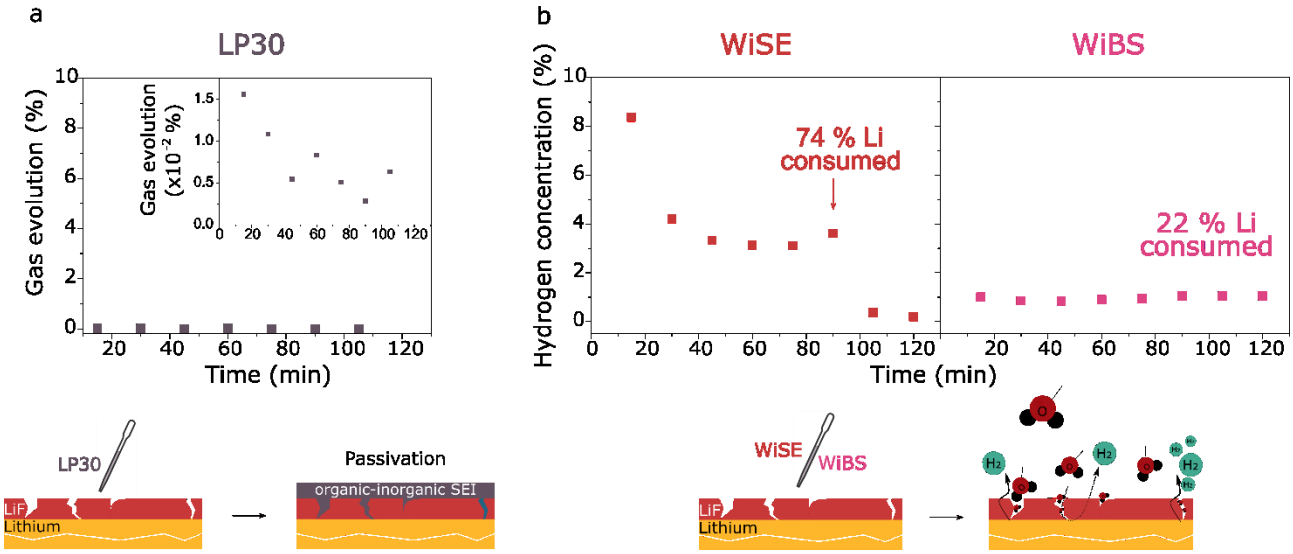

Figure 3 (a) Gas evolution as a function of time for LiF-protected metallic Li samples during exposure to EC:DMC 1M $LiPF_6$ (LP30) and schematic illustration of SEI behavior. The gas evolution is the sum of all gases detected (see Supporting information for detailed measurements). (b) Hydrogen evolution as a function of time for LiF-protected metallic Li samples upon exposure to 20 m LiTFSI (WiSE) and 20 m LiTFSI : 8 m LiBETI (WiBS) aqueous superconcentrated electrolytes.

In contrast, a large amount of hydrogen (≈ 8 %) is detected in the sampled gas with a LiF-protected metallic Li sample exposed to 20 m LiTFSI electrolyte (Figure 3b). This amount then stabilizes at ≈ 4% before vanishing after 100 minutes when almost all the metallic Li is consumed (≈ 80%, see Table S4). Similarly, when exposing the LiF-protected Li sample to 20 m LiTFSI : 8 m LiBETI, hydrogen is detected with a concentration of ≈ 1 %. Unlike for the 20 m LiTFSI solution, this concentration remains constant throughout the measurement, leading to a consumption of ≈ 22 % of metallic Li after 2 hours (see Table S5). Eventually, such continuous hydrogen evolution indicates that, unlike for carbonate-based electrolytes, no self-passivation occurs in superconcentrated aqueous electrolytes. Altogether, these GC-TCD results indicate that aqueous electrolyte reaches the underneath metallic Li electrode through microstructural defects, i.e. cracks or grain boundaries, which have previously being observed for native SEI formed in superconcentrated aqueous electrolytes by SEM and TEM experiments [1,5,20,21]. As the kinetics for water reduction is not drastically impacted by the salt concentration[7] and knowing that the quantity of water contained in 250 µL of aqueous superconcentrated electrolytes does not limit the reaction (see Table S 2 and Table S 3 in Supporting Information), one can hypothesize that the greater the viscosity of the electrolyte, (η_{WiBS} = 203 mPa at 30 °C [2] and η_{WiSE} = 36.2 mPa at 25 °C [1]), the slower the electrolyte penetrates through minute cracks present in the LiF layer, thus explaining the differences of Li-water reactivity between the two superconcentrated aqueous electrolytes.

One legitimate question arising from this study regards the quality of the LiF layer. We thus compared the protective power of our LiF layer with that of a conformal Al_2O_3 layer prepared by atomic layer deposition (ALD), previously proposed to allow for passivating anode materials in WiSE as Al_2O_3 is not soluble in water [22,23]. Using a similar approach combining E-SEM and GC-TCD (see Figure S4a and b), evolution of hydrogen upon consumption of the underlying Li electrode is once

again observed (see Table S6). To summarize, acknowledging that the high-quality LiF layer prepared in this work, as well as Al_2O_3 prepared by ALD deposition method, will always exhibit some degree of structural defects (cracks, microporosity or else) alike a native SEI which consists of a mosaic of LiF grains [1,10] (and which can further be introduced upon cycling the electrode), our study highlights that even if the use of superconcentrated aqueous electrolytes prevents the dissolution of the inorganic SEI compounds, these electrolytes are deprived of self-passivating ability through the formation of a polymeric SEI outer layer required to stabilize anode materials.

To overcome the absence of self-passivation, LiF-protected Li samples were soaked in 50 µL of three organic-based solutions: pure fluoro-ethylene carbonate (FEC) solvent and two electrolytes, namely 7 M LiFSI in FEC and 2 M LiFSI : 1 M LiTFSI in a mixture of 1,3-dioxolane: 1,2-dimethoxyethane (DOL/DME) with 3 % $LiNO_3$ additive, both known for forming good elastomeric passivating SEI with an LiF-rich inner layer, enabling high Coulombic efficiencies for Li plating/striping [24–26]. After soaking, during which any possible defects within the LiF layer can be further passivated by the formation of an additional organic-inorganic layer derived from a non-aqueous electrolyte, the samples are exposed to superconcentrated aqueous electrolyte (Figure 4a). Figure 4b shows the hydrogen concentration measured over time for these three samples exposed to WiBS. First, the hydrogen concentration measured after pre-soaking the sample in pure FEC is similar than for the pristine LiF-protected Li sample. Interestingly, when increasing the volume of FEC during the soaking step (from 50 µL to 2 mL), we observe an increase of hydrogen evolution (≈ 3 % after 15 min compared to ≈ 1 % for the pristine Li/LiF as shown in Figure S 6a). Combining this observation with post soaking XPS analysis, we demonstrate that this can be attributed to the partial dissolution of the LiF layer in FEC (Figure S 6b and c).

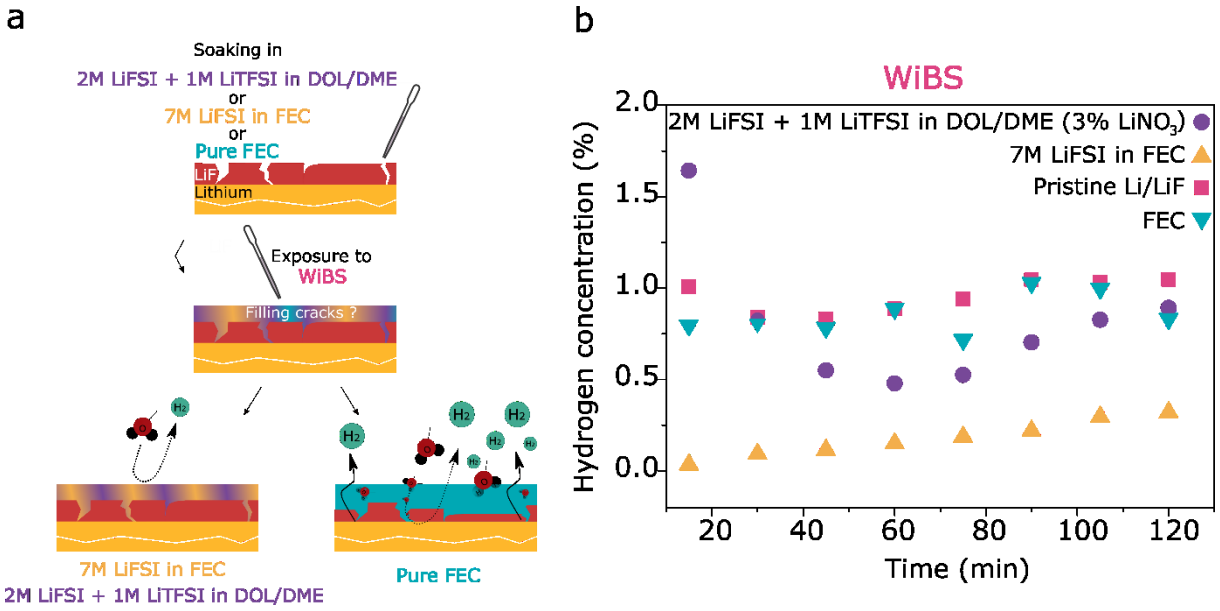

Figure 4*:* a. Schematic representation of the LiF-coated metallic Li behavior after pre-soaking in organic electrolyte and exposure to WiBS. b. Hydrogen evolution as function of time for Li/LiF sample pristine Li/LiF (pink), Li/LiF pre-soaked in in pure FEC (light blue), Li/LiF pre-soaked in 7 M LiFSI in FEC (yellow) or pre-soaked in 2 M LiFSI : 1 M LiTFSI in DOL/DME (purple) prior to exposure to 20 m LiTFSI : 8 m LiBETI aqueous superconcentrated electrolyte (WiBS).

To overcome the dissolution of the LiF coating, samples were then soaked in an ether-based electrolyte (1 M LiTFSI : 2 M LiFSI in DOL/DME + 3% $LiNO_3$). When exposing this sample to WiBS (Figure 4a), the hydrogen evolution is greater after 15 min (≈ 1.6 %) than for the pristine LiF-protected Li sample. Nevertheless, the signal rapidly decreases and stabilizes below 1 % of hydrogen detected in the headspace. Overall, after this equilibration period, soaking the LiF-protected Li anode in 1 M LiTFSI : 2 M LiFSI in DOL/DME + 3% $LiNO_3$ has a slight positive impact on the gassing, decreasing the Li consumption through hydrogen evolution by 4 % when compared with the pristine Li/LiF sample.

Having shown that avoiding dissolution of the artificial LiF-based SEI is crucial, we then soaked a fresh sample in an organic superconcentrated electrolyte, namely 7 M LiFSI in FEC, before exposing it to WiBS (Figure 4a). This soaking step is found to have a beneficial impact and diminishes the

hydrogen evolution upon exposure to WiBS, which approaches the detection limit even at the earlier stage of exposure (0.035 % of the total headspace after 15 min). Furthermore, even if the amount of hydrogen detected slightly increases with time, it corresponds to a consumption of Li of only 4 % after 2 hours considering HER as the sole source for H_2 evolution, compared to 22 % for the pristine LiF-protected Li sample.

One can suspect that the beneficial impact of 7 M LiFSI in FEC and 1 M LiTFSI : 2 M LiFSI in DOL/DME + $LiNO_3$ arises from their ability to form an inorganic-organic SEI upon decomposition on the surface of Li,[17,28] both being able to partially compensate the microstructural defects of the *ex-situ* LiF interface. Indeed, as shown Figure S 7, post soaking XPS analysis reveal the formation of a salt-derived inorganic SEI for both electrolytes as well as an organic SEI outer layer for the DOL/DME-based electrolyte. Besides, similar experiments have been performed in WiSE (see Figure S 3). As in WiBS, the soaking in 1 M LiTFSI : 2 M LiFSI in DOL/DME + 3% $LiNO_3$ and in 7 M LiFSI FEC has a beneficial, but reduced, impact on the hydrogen gassing.

Consequently, the beneficial impact on hydrogen gassing when a LiF-coated Li sample is exposed to WiBS ranks as follows: pristine Li/LiF < pure FEC < 1 M LiTFSI : 2 M LiFSI in DOL/DME + 3% $LiNO_3$ < 7 M LiFSI in FEC. From this trend, one can conclude that the ability of the electrolyte to form and maintain stable a LiF-rich SEI inner layer is of prime importance to positively stabilize the interface. Additionally, forming an organic SEI outer layer, as we observe for DOL/DME, tends to be beneficial as recently demonstrated with the use of organic co-solvents such as acetonitrile [29], DMC [30,31] or ether-based one (TEGDME)[32]. Similarly, additives such as urea [33,34] were also shown to have positive effects on the cycling behavior of $Li_4Ti_5O_{12}$ anode (1.7 V *vs* Li^+/Li) in WiSE-based batteries owing to its decomposition in both inorganic (Li_2CO_3) and amorphous organic (polyuria) layers. Nevertheless, bearing in mind that in these electrolytes, the first solvation sheath of Li contains both water and organic species, it is tempting to conclude that both should be simultaneously present at the

interface, leading to the detrimental reduction of water simultaneously to the SEI formation knowing that solvating water molecules are more reactive than non-solvating ones [35].

Moreover, despite the diminished hydrogen evolution with an artificial inorganic LiF layer pre-soaked in 7 M LiFSI in FEC, these *ex-situ* protections are not sufficient to envision practical applications. Indeed, considering the electrolyte's water content as the limiting factor, in the best-case scenario, fewer than 50 cycles in WiSE and 250 cycles in WiBS would be achieved before the drying out of a cell cycled at 1C C-rate (see Table S 7). Furthermore, taking into account the quantity of Li used in this study (489 µmol), only 6 h would be needed to fully consume Li in WiSE, and less than 50 h in WiBS. These simple calculations do not take into account electrolyte crystallization but merely the full consumption of water, thus providing grossly underestimated numbers that would be even worse in practice. Evidently, using Li as an anode leads to harsh degradation which could be partially alleviated, or at least slowed down, by the use of an anode material with a greater redox potential ($Li_4Ti_5O_{12}$, TiO_2, Mo_6S_8, $LiTi_2(PO_4)_3$ or else). Indeed, around 8750 cycles could be performed using unprotected Mo_6S_8 as negative electrode before the complete drying out of the cell [13], this gain in cycling life coming at the expense of energy density.

Altogether, this work evidences that 1) the use of superconcentrated aqueous electrolytes does not allow for the self-passivation of the SEI at the anode; 2) the solubility is not the predominant factor governing the poor stability of such inorganic coatings; and 3) while inorganic-rich interphases can physically impede the reaction and allow for a certain stability over a short period of time, the aqueous electrolyte will inherently reaches the underlying anode material owing to extrinsic defects which will be present in any practical the SEI. Furthermore, bearing in mind that cracks and/or microporosity may continuously form upon cycling, triggering their self-passivation is necessary to protect the underneath electrode. Towards that goal, two strategies can be envisioned, either through the use of additives or of organic coatings. Regarding the use of additives, they must be

targeted following their ability to preferentially solvate Li^+ and thus displace water from its solvation sheath. Organic coatings can also be developed by a grafting strategy or by laminating polymer protective layers, as previously reported[36,37]. Nevertheless, when conducting such exploratory studies, the reactivity of the underlying negative electrode must be accurately measured, using slow cycling as well as self-discharge cycles. Only the coupling of such a chemical approaches with proper electrochemical characterizations sustain a chance at achieving the long-lasting goal of developing stable SEI layers for aqueous electrochemical systems.

Materials and methods

Sample preparation

- *LiF*

LiF coating of approximately 30nm thickness were deposited onto Li following the reaction of NF_3 with metallic Li (NF_3 + 3 Li → 3 LiF + ½ N_2) at 175 °C for 1 h as described in He *et al.* [17] . Current collectors were made of stainless steel (SS). SS/Li/LiF samples were 1.27 cm in diameter for E-SEM, SEM and XRD experiments. SS/Li/LiF samples were 0.9 cm in diameter for GC-TCD tests.

- *Al_2O_3*

Al_2O_3 coating of thicknesses comprised between 2 and 10 nm were deposited by ALD (atomic layer deposition). The Al_2O_3 layers were deposited on the top of Li metal samples by ALD using a Picosun R-200 Advanced reactor which is a hot wall, flow through type reaction chamber operating in thermal ALD mode using O_3 (ozone) deposition process. The AC series (AC-bench 2025) ozone generator offers state-of-the-art silent corona discharge ozone generating technology based on 0_2 (99.5 %) / N_2 (0.5 %) mixing gas. The deposition temperature range was set to 140 °C, i.e. at a threshold level well below the Li melting temperature (~ 180 °C). Trimethylaluminium (TMA) served

as precursor (δt_{TMA} = 0.1 s) and O_3 (δt_{O3} = 0.6 s) as reactant (second precursor) to achieve the deposition of homogenous and conformal Al_2O_3 layers (2 to 10 nm-thick).

- *Electrolyte preparation*

Lithium bis(trifluoromethanesulfonyl)imide (LiTFSI, 99.9% Extra-dry, 20ppm max., $LiN(SO_2CF_3)_2$) was purchased from Solvionic and used as received. Lithium bis(pentafluoroethanesulfonyl)imide (LiBETI, 98%, $LiN(SO_2CF_2CF_3)_2$ and lithium bis(fluorosulfonyl)imide (LiFSI, 98%, $LiN(SO_2F)_2$) were purchased from TCI Chemicals and used as received. Lithium nitrate ($LiNO_3$, 99%) was purchased from Alfa Aesar and used as received.

-Aqueous electrolytes:

1 mol / kg LiTFSI, 3 mol / kg LiTFSI, 5 mol / kg LiTFSI, 7 mol / kg LiTFSI, 10 mol / kg LiTFSI, 15 mol / kg LiTFSI, 20 mol / kg LiTFSI, 20 mol / kg LiTFSI: 8 mol /kg LiBETI electrolyte solutions were prepared by mixing Milli-Q ultrapure water and the corresponding amount of salt.

-Organic electrolytes:

Pure organic solvents EC (Ethylene carbonate) and DMC (Dimethyl carbonate), 1,3-dioxolane (DOL), 1,2-dimethoxyethane (DME) were purchased from Sigma. Fluoroethylene carbonate (FEC) was purchased from TCI Chemicals. EC:DMC (1:1 vol%) and DOL:DME (1:1 vol%) were prepared by mixing the appropriate solvents. All pure solvents were dried over molecular sieve prior to be used for solubility measurements. EC:DMC (1:1 %vol) from Dodochem was used to perform the organic calibration of the ISE (Ion selective electrode). To prepare non-aqueous electrolytes (7M LiFSI in FEC, 1M LiTFSI : 2M LiFSI in DOL:DME + 3% $LiNO_3$), salts were dried in a vacuum oven at 110 °C prior to mixing and the electrolytes were dried over molecular sieves before use.

<u>Characterizations</u>

- *Solubility limit measurements: Ion selective electrode (ISE) to Fluoride*

To determine the solubility limit of fluoride in both aqueous and organic-based solution, a fluoride ISE from Hach Lang (Intellical, ISEF121) was used. Prior to any solubility measurements, the electrode was calibrated using the following protocol:

-Aqueous standard preparation

Standard aqueous solutions (25 mL minimum) were prepared by dissolving sodium fluoride (NaF, Alfa Aesar) in pure mQ-water at a concentration of 1000 mg / L. By dilution of a factor 10, solutions of concentration 100 mg / L; 10 mg / L; 1 mg / L; 0.1 mg / L; 0.01 mg / L were prepared. One pillow of fluoride ionic strength buffer (TISAB, Hach) was added to each standard to perform the measurements.

-Organic standard preparation

Organic standard solutions were prepared by dilution of 1 mol / L of TBAF in THF solution (tetrabutylammonium fluoride solution, 1.0 M in THF, Sigma) in EC:DMC (Dodochem, 1:1 vol%) at a concentration of fluoride of 1900 mg / L. By continuous dilution, standards with lower concentration were prepared. The organic standards were then diluted in an TISAB:H_2O (1 TISAB pillow for 20 mL mQ-water) aqueous solution to perform the experiments. Doing so, the organic standards were diluted by a factor 11 by adding 2 mL of the organic standard to 20 mL of TISAB:H_2O solution. Eventually, the following standard concentrations were prepared: 157 mg / L; 14 mg / L; 1.30 mg / L; 0.12 mg / L and 0.011 mg / L.

The potential and the temperature of the standard solutions were recorded by the F^- ISE under stirring in a plastic beaker. The calibration curve obtained in both aqueous and organic media are presented in *Figure S 1*.

A slope of -55.8 mV / decade is obtained at 23 °C in aqueous standards while slope of -53.8 mV / decade is found in organic standard at 23 °C. The theoretical slope is -58.7 mV / decade, and both calibrations were considered to be sufficiently accurate to perform LiF solubility measurements.

Commercial lithium fluoride (LiF powder, 300 mesh, Sigma Aldrich) was used in solubility tests. Saturated solutions were prepared as follows: excess amount of LiF were added to the solution (see the list in Sample preparation, Electrolyte preparation). The solution was (i) let to stir at least overnight at constant temperature and (ii) let to rest before the formation of a precipitate could be visually observed. The solution was then centrifuged for 10 min at 6000 tr / min and the supernatant filtered using a PTFE or a polypropylene 0.2 µm pores filter. Solubility limit measurements were performed at the thermodynamic equilibrium. Therefore, we do not expect the solubility measurements to be dependent on the particulate size neither on their morphologies. Moreover, superconcentrated aqueous electrolyte were reported to be acidic[38]. Our solubility measurements take into account this effect and its potential impact on the LiF solubility. Regarding the samples measured at 55°C, all the laboratory equipments (pipettes, centrifuge tube, filter etc.) used were previously heated at 55°C to avoid temperature artefacts. 2 mL of the saturated solutions were then diluted in 20 mL of milli-Q ultrapure water to prepare a diluted LiF-saturated electrolyte. Once the dilution was performed, the LiF concentration in solution is far from the solubility limit, therefore temperature control was unnecessary.

Low-level measurements were conducted according to the following protocol: a TISAB pillow was added to 25 mL of milli-Q ultrapure water. 5 mL of the as-prepared solution was added to the diluted LiF-saturated electrolyte. The solution was stirred and [F^-] was measured. Three measurements were performed for each sample tested, except for 20 m LiTFSI : 8 m LiBETI. The mean value and standard deviation (3σ) are shown.

- SEM *(Scanning electron microscopy) imaging*

Scanning electron microscopy (SEM) images of Li/LiF samples were taken with a Zeiss Merlin scanning electron microscope at an accelerating voltage of 1 kV. Samples were transferred to the SEM without exposure to air via a transfer vessel (Semilab Inc.) built for the Zeiss SEM airlock. The

average and standard deviation of the LiF layer thickness were determined by measurements at five random positions on the edge of LiF layer in the cross-section view with tilt angle correction.

- *E-SEM (Environmental scanning electron microscopy) imaging*

Li, Li/LiF and Li/Al_2O_3 samples of 1.27 cm, 1.27 cm and 0.7 cm in diameter, respectively, are affixed to sample holders using Cu tape in an Ar-filled glovebox (< 0.1 ppm O_2, < 0.1 ppm H_2O). The samples are transferred from the Ar-filled glovebox to an environmental SEM (ESEM Quattro S by Thermo Fisher Scientific) with minimal exposure to air and loaded into the chamber under high vacuum. The SEM is used in high-vacuum (0 % relative humidity, RH) and environmental (5, 30, 45, 60, 75 and 90 % RH) mode for SEM imaging at 20 °C with a GSED detector in secondary electron (topography) mode. After recording a reference image at 0 % RH in high-vacuum mode (left-most images in Figure 1b), the SEM is operated in ESEM mode at 5 % RH. The samples are then exposed to 15 % RH for 2 minutes and imaged at 5 % RH; alternating between reaction (high RH for 2 minutes) and imaging (always 5 % RH) conditions is repeated for 30, 45, 60, 75 and 90 % RH (see depiction of samples exposed to 30, 60 and 90 % RH and imaged at 5 % RH in Fig. 1b). The SEM images are taken at 1.5/1.8 nA and 10/15 kV at a working distance of 8 mm, and a resolution of 1536 x 1024 pixel with a horizontal field width of 207 µm.

- Gas chromatography

The gas measurements were performed using the following procedure:

Inside an Ar-filled glovebox (< 0.1 ppm O_2, < 0.1 ppm H_2O), a gas-tight cell made from chemically-inert polyetheretherketone (PEEK) was assembled with Li/LiF or Al_2O_3 samples inside. The cell has a 5.5 mL gas headspace, inlet and outlet valves, and septa through which liquids can be injected and gas from the headspace can be extracted with gas-tight syringe. The gas-tight cell was then taken outside of the glovebox, connected to an Ar tank (R300, Airgas) and purged for 5 min at 100 mg_{Ar}/min. The cell was then filled with Ar to a pressure of 30 psi. 250 µL of electrolyte (20 m LiTFSI

or 20 m LiTFSI : 8 m LiBETI) was then injected into the cell through a septum with a gas-tight syringe. Every 15 min, a 2.5 mL gas sample was collected with a gas-tight syringe and the remaining Ar headspace was purged with fresh Ar at 100 mg_{Ar}/min for 1 minute and the pressure set back to 30 psi. The gas sample were then injected into an Agilent 7890B gas chromatography instrument equipped with thermal conductivity (TCD) and flame ionization (FID) detectors for gas analysis, calibrated using 15 ppm and 1 vol% gas standards in N_2 (Supelco). The TCD detector was used for H_2 and CO_2 quantification, and the FID detector was used for CH_4, C_2H_2, C_2H_4, C_2H_6 and CO quantification.

The pre-soaking of the LiF-coated samples was done by pipetting 50 µL of the organic electrolytes on LiF-coated Li samples inside a glovebox, which was left to react for 1 h, and subsequently dried under antechamber vacuuum for 1 h before exposure to aqueous superconcentrated electrolytes. As the exposure to organic FSI^--based electrolytes lasts one hour followed by a one-hour drying step, FSI^- is not directly exposed to water. If so, the time during which (two hours) the remaining traces of FSI^- anions may be exposed to either WiSE or WiBS is far shorter than the time necessary to detect a significant FSI^- hydrolysis [27].

- XPS

X-ray photoelectron spectroscopy (XPS) was conducted on a PHI VersaProbe II X-ray Photoelectron Spectrometer. Samples were transferred to XPS in an air-sensitive transfer vessel to minimize exposure to air. Binding energies were calibrated by the adventitious carbon peak at 284.8 eV.

Supporting Information

The Supporting Information is available free of charge at the ACS Publication website at DOI: XXXX. The Supporting Information contain calibration curves and further analysis for the solubility measurements, SEM images for the LiF-coatings, environmental SEM and GC-TCD measurements

for Al_2O_3 coatings, further GC-TCD and XPS measurements for LiF coatings as well as estimation for water and lithium consumption.

Author Information

Authors contributed equally: L.D., G.M.H.

Corresponding Author:

Alexis Grimaud (alexis.grimaud@college-de-france.fr)

Betar M. Gallant (bgallant@mit.edu)

The authors declare no conflict of interest

Acknowledgment, Funding

L.D. would like to acknowledge the Direction Générale de l'Armement (DGA) for financial support. The authors would like to thank the French National Research Agency for its support through the Labex STORE-EX project (ANR-10-LABX-76-01) and through the project BALWISE (project ID: ANR-19-CE05-0014). R.G. gratefully acknowledges support from the National Science Foundation under award number 1804247. This work made use of the MRSEC Shared Experimental Facilities at MIT, supported by the National Science Foundation under award number DMR-1419807.

References

(1) Suo, L.; Borodin, O.; Gao, T.; Olguin, M.; Ho, J.; Fan, X.; Luo, C.; Wang, C.; Xu, K. "Water-in-Salt" Electrolyte Enables High-Voltage Aqueous Lithium-Ion Chemistries. *Science* **2015**, *350* (6263), 938–943. https://doi.org/10.1126/science.aab1595.

(2) Yamada, Y.; Usui, K.; Sodeyama, K.; Ko, S.; Tateyama, Y.; Yamada, A. Hydrate-Melt Electrolytes for High-Energy-Density Aqueous Batteries. *Nat. Energy* **2016**, *1* (10), 16129. https://doi.org/10.1038/nenergy.2016.129.

(3) Wang, X.; Qu, Q.; Hou, Y.; Wang, F.; Wu, Y. An Aqueous Rechargeable Lithium Battery of High Energy Density Based on Coated Li Metal and LiCoO2. *Chem. Commun.* **2013**, *49* (55), 6179. https://doi.org/10.1039/c3cc42676a.

(4) Suo, L.; Borodin, O.; Wang, Y.; Rong, X.; Sun, W.; Fan, X.; Xu, S.; Schroeder, M. A.; Cresce, A. V.; Wang, F.; Yang, C.; Hu, Y.-S.; Xu, K.; Wang, C. "Water-in-Salt" Electrolyte Makes Aqueous Sodium-Ion Battery

Safe, Green, and Long-Lasting. *Adv. Energy Mater.* **2017**, *7* (21), 1701189. https://doi.org/10.1002/aenm.201701189.

(5) Suo, L.; Borodin, O.; Sun, W.; Fan, X.; Yang, C.; Wang, F.; Gao, T.; Ma, Z.; Schroeder, M.; von Cresce, A.; Russell, S. M.; Armand, M.; Angell, A.; Xu, K.; Wang, C. Advanced High-Voltage Aqueous Lithium-Ion Battery Enabled by "Water-in-Bisalt" Electrolyte. *Angew. Chem. Int. Ed.* **2016**, *55* (25), 7136–7141. https://doi.org/10.1002/anie.201602397.

(6) Suo, L.; Oh, D.; Lin, Y.; Zhuo, Z.; Borodin, O.; Gao, T.; Wang, F.; Kushima, A.; Wang, Z.; Kim, H.-C.; Qi, Y.; Yang, W.; Pan, F.; Li, J.; Xu, K.; Wang, C. How Solid-Electrolyte Interphase Forms in Aqueous Electrolytes. *J. Am. Chem. Soc.* **2017**, *139* (51), 18670–18680. https://doi.org/10.1021/jacs.7b10688.

(7) Dubouis, N.; Lemaire, P.; Mirvaux, B.; Salager, E.; Deschamps, M.; Grimaud, A. The Role of the Hydrogen Evolution Reaction in the Solid–Electrolyte Interphase Formation Mechanism for " *Water-in-Salt* " Electrolytes. *Energy Environ. Sci.* **2018**, *11* (12), 3491–3499. https://doi.org/10.1039/C8EE02456A.

(8) Steinrück, H.; Cao, C.; Lukatskaya, M. R.; Takacs, C. J.; Wan, G.; Mackanic, D. G.; Tsao, Y.; Zhao, J.; Helms, B. A.; Xu, K.; Borodin, O.; Wishart, J. F.; Toney, M. F. Interfacial Speciation Determines Interfacial Chemistry: X-ray-Induced Lithium Fluoride Formation from Water-in-salt Electrolytes on Solid Surfaces. *Angew. Chem. Int. Ed.* **2020**, anie.202007745. https://doi.org/10.1002/anie.202007745.

(9) Ko, S.; Yamada, Y.; Yamada, A. Formation of a Solid Electrolyte Interphase in Hydrate-Melt Electrolytes. *ACS Appl. Mater. Interfaces* **2019**, acsami.9b13662. https://doi.org/10.1021/acsami.9b13662.

(10) Peled, E.; Golodnitsky, D.; Ardel, G. Advanced Model for Solid Electrolyte Interphase Electrodes in Liquid and Polymer Electrolytes. *J. Electrochem. Soc.* **1997**, *144* (8), L208–L210. https://doi.org/10.1149/1.1837858.

(11) Gauthier, M.; Carney, T. J.; Grimaud, A.; Giordano, L.; Pour, N.; Chang, H.-H.; Fenning, D. P.; Lux, S. F.; Paschos, O.; Bauer, C.; Maglia, F.; Lupart, S.; Lamp, P.; Shao-Horn, Y. Electrode–Electrolyte Interface in Li-Ion Batteries: Current Understanding and New Insights. *J. Phys. Chem. Lett.* **2015**, *6* (22), 4653–4672. https://doi.org/10.1021/acs.jpclett.5b01727.

(12) Kühnel, R.-S.; Reber, D.; Battaglia, C. Perspective—Electrochemical Stability of Water-in-Salt Electrolytes. *J. Electrochem. Soc.* **2020**, *167* (7), 070544. https://doi.org/10.1149/1945-7111/ab7c6f.

(13) Droguet, L.; Grimaud, A.; Fontaine, O.; Tarascon, J. Water-in-Salt Electrolyte (WiSE) for Aqueous Batteries: A Long Way to Practicality. *Adv. Energy Mater.* **2020**, *10* (43), 2002440. https://doi.org/10.1002/aenm.202002440.

(14) Jones, J.; Anouti, M.; Caillon-Caravanier, M.; Willmann, P.; Lemordant, D. Thermodynamic of LiF Dissolution in Alkylcarbonates and Some of Their Mixtures with Water. *Fluid Phase Equilibria* **2009**, *285* (1–2), 62–68. https://doi.org/10.1016/j.fluid.2009.07.020.

(15) Strmcnik, D.; Castelli, I. E.; Connell, J. G.; Haering, D.; Zorko, M.; Martins, P.; Lopes, P. P.; Genorio, B.; Østergaard, T.; Gasteiger, H. A.; Maglia, F.; Antonopoulos, B. K.; Stamenkovic, V. R.; Rossmeisl, J.; Markovic, N. M. Electrocatalytic Transformation of HF Impurity to H2 and LiF in Lithium-Ion Batteries. *Nat. Catal.* **2018**, *1* (4), 255–262. https://doi.org/10.1038/s41929-018-0047-z.

(16) McEldrew, M.; Goodwin, Z. A. H.; Bi, S.; Bazant, M. Z.; Kornyshev, A. A. Theory of Ion Aggregation and Gelation in Super-Concentrated Electrolytes. *J. Chem. Phys.* **2020**, *152* (23), 234506. https://doi.org/10.1063/5.0006197.

(17) He, M.; Guo, R.; Hobold, G. M.; Gao, H.; Gallant, B. M. The Intrinsic Behavior of Lithium Fluoride in Solid Electrolyte Interphases on Lithium. *Proc. Natl. Acad. Sci.* **2020**, *117* (1), 73–79. https://doi.org/10.1073/pnas.1911017116.

(18) Aurbach, D.; Ein-Ely, Y.; Zaban, A. The Surface Chemistry of Lithium Electrodes in Alkyl Carbonate Solutions. *J. Electrochem. Soc.* **1994**, *141* (1), L1–L3. https://doi.org/10.1149/1.2054718.

(19) Guo, R.; Wang, D.; Zuin, L.; Gallant, B. M. Reactivity and Evolution of Ionic Phases in the Lithium Solid–Electrolyte Interphase. *ACS Energy Lett.* **2021**, *6* (3), 877–885. https://doi.org/10.1021/acsenergylett.1c00117.

(20) Liu, D.; Yu, Q.; Liu, S.; Qian, K.; Wang, S.; Sun, W.; Yang, X.-Q.; Kang, F.; Li, B. Evolution of Solid Electrolyte Interface on TiO_2 Electrodes in an Aqueous Li-Ion Battery Studied Using Scanning

Electrochemical Microscopy. *J. Phys. Chem. C* **2019**, acs.jpcc.9b01412. https://doi.org/10.1021/acs.jpcc.9b01412.

(21) Zhang, H.; Wang, D.; Shen, C. In-Situ EC-AFM and Ex-Situ XPS Characterization to Investigate the Mechanism of SEI Formation in Highly Concentrated Aqueous Electrolyte for Li-Ion Batteries. *Appl. Surf. Sci.* **2020**, *507*, 145059. https://doi.org/10.1016/j.apsusc.2019.145059.

(22) Chen, L.; Cao, L.; Ji, X.; Hou, S.; Li, Q.; Chen, J.; Yang, C.; Eidson, N.; Wang, C. Enabling Safe Aqueous Lithium Ion Open Batteries by Suppressing Oxygen Reduction Reaction. *Nat. Commun.* **2020**, *11* (1), 2638. https://doi.org/10.1038/s41467-020-16460-w.

(23) Wang, F.; Lin, C.-F.; Ji, X.; Rubloff, G. W.; Wang, C. Suppression of Hydrogen Evolution at Catalytic Surfaces in Aqueous Lithium Ion Batteries. *J. Mater. Chem. A* **2020**, *8* (30), 14921–14926. https://doi.org/10.1039/D0TA05568A.

(24) Zhang, X.-Q.; Cheng, X.-B.; Chen, X.; Yan, C.; Zhang, Q. Fluoroethylene Carbonate Additives to Render Uniform Li Deposits in Lithium Metal Batteries. *Adv. Funct. Mater.* **2017**, *27* (10), 1605989. https://doi.org/10.1002/adfm.201605989.

(25) Aurbach, D. A Short Review of Failure Mechanisms of Lithium Metal and Lithiated Graphite Anodes in Liquid Electrolyte Solutions. *Solid State Ion.* **2002**, *148* (3–4), 405–416. https://doi.org/10.1016/S0167-2738(02)00080-2.

(26) Li, C.; Lan, Q.; Yang, Y.; Shao, H.; Zhan, H. Flexible Artificial Solid Electrolyte Interphase Formed by 1,3-Dioxolane Oxidation and Polymerization for Metallic Lithium Anodes. *ACS Appl. Mater. Interfaces* **2019**, *11* (2), 2479–2489. https://doi.org/10.1021/acsami.8b16080.

(27) Reber, D.; Figi, R.; Kühnel, R.-S.; Battaglia, C. Stability of Aqueous Electrolytes Based on LiFSI and NaFSI. *Electrochimica Acta* **2019**, *321*, 134644. https://doi.org/10.1016/j.electacta.2019.134644.

(28) Suo, L.; Xue, W.; Gobet, M.; Greenbaum, S. G.; Wang, C.; Chen, Y.; Yang, W.; Li, Y.; Li, J. Fluorine-Donating Electrolytes Enable Highly Reversible 5-V-Class Li Metal Batteries. *Proc. Natl. Acad. Sci.* **2018**, *115* (6), 1156–1161. https://doi.org/10.1073/pnas.1712895115.

(29) Chen, J.; Vatamanu, J.; Xing, L.; Borodin, O.; Chen, H.; Guan, X.; Liu, X.; Xu, K.; Li, W. Improving Electrochemical Stability and Low-Temperature Performance with Water/Acetonitrile Hybrid Electrolytes. *Adv. Energy Mater.* **2020**, *10* (3), 1902654. https://doi.org/10.1002/aenm.201902654.

(30) Wang, F.; Borodin, O.; Ding, M. S.; Gobet, M.; Vatamanu, J.; Fan, X.; Gao, T.; Eidson, N.; Liang, Y.; Sun, W.; Greenbaum, S.; Xu, K.; Wang, C. Hybrid Aqueous/Non-Aqueous Electrolyte for Safe and High-Energy Li-Ion Batteries. *Joule* **2018**, *2* (5), 927–937. https://doi.org/10.1016/j.joule.2018.02.011.

(31) Wrogemann, J. M.; Künne, S.; Heckmann, A.; Rodríguez-Pérez, I. A.; Siozios, V.; Yan, B.; Li, J.; Winter, M.; Beltrop, K.; Placke, T. Development of Safe and Sustainable Dual-Ion Batteries Through Hybrid Aqueous/Nonaqueous Electrolytes. *Adv. Energy Mater.* **2020**, *10* (8), 1902709. https://doi.org/10.1002/aenm.201902709.

(32) Shang, Y.; Chen, N.; Li, Y.; Chen, S.; Lai, J.; Huang, Y.; Qu, W.; Wu, F.; Chen, R. An "Ether-In-Water" Electrolyte Boosts Stable Interfacial Chemistry for Aqueous Lithium-Ion Batteries. *Adv. Mater.* **2020**, *32* (40), 2004017. https://doi.org/10.1002/adma.202004017.

(33) Hou, Z.; Dong, M.; Xiong, Y.; Zhang, X.; Zhu, Y.; Qian, Y. Formation of Solid–Electrolyte Interfaces in Aqueous Electrolytes by Altering Cation-Solvation Shell Structure. *Adv. Energy Mater.* **2020**, *10* (15), 1903665. https://doi.org/10.1002/aenm.201903665.

(34) Zhang, X.; Dong, M.; Xiong, Y.; Hou, Z.; Ao, H.; Liu, M.; Zhu, Y.; Qian, Y. Aqueous Rechargeable Li^+/Na^+ Hybrid Ion Battery with High Energy Density and Long Cycle Life. *Small* **2020**, *16* (41), 2003585. https://doi.org/10.1002/smll.202003585.

(35) Dubouis, N.; Serva, A.; Salager, E.; Deschamps, M.; Salanne, M.; Grimaud, A. The Fate of Water at the Electrochemical Interfaces: Electrochemical Behavior of Free Water Versus Coordinating Water. *J Phys Chem Lett* **2018**, 6683-6688.
https://doi.org/10.1021/acs.jpclett.8b03066.

(36) Alloin, F.; Crepel, L.; Cointeaux, L.; Leprêtre, J.-C.; Fusalba, F.; Martinet, S. The Interest of Diazonium Chemistry for Aqueous Lithium-Ion Battery. *J. Electrochem. Soc.* **2013**, *160* (5), A3171–A3178. https://doi.org/10.1149/2.026305jes.

(37) Yang, C.; Chen, J.; Qing, T.; Fan, X.; Sun, W.; von Cresce, A.; Ding, M. S.; Borodin, O.; Vatamanu, J.; Schroeder, M. A.; Eidson, N.; Wang, C.; Xu, K. 4.0 V Aqueous Li-Ion Batteries. *Joule* **2017**, *1* (1), 122–132. https://doi.org/10.1016/j.joule.2017.08.009.

(38) Han, K. S.; Yu, Z.; Wang, H.; Redfern, P. C.; Ma, L.; Cheng, L.; Chen, Y.; Hu, J. Z.; Curtiss, L. A.; Xu, K.; Murugesan, V.; Mueller, K. T. Origin of Unusual Acidity and Li^+ Diffusivity in a Series of Water-in-Salt Electrolytes. *J. Phys. Chem. B* **2020**, *124* (25), 5284–5291. https://doi.org/10.1021/acs.jpcb.0c02483.